Direct Detection of Electron Backscatter Diffraction Patterns

Angus J. Wilkinson,[1] Grigore Moldovan,[1,*] T. Benjamin Britton,[1,3] Angus Bewick,[2]
Robert Clough,[1] and Angus I. Kirkland[1]

[1]Department of Materials, University of Oxford, Parks Road, Oxford OX1 3PH, United Kingdom
[2]Oxford Instruments, Halifax Road, High Wycombe HP12 3SE, United Kingdom
[3]Department of Materials, Imperial College London, London SW7 2AZ, United Kingdom

(Received 30 April 2013; published 8 August 2013)

We report the first use of direct detection for recording electron backscatter diffraction patterns. We demonstrate the following advantages of direct detection: the resolution in the patterns is such that higher order features are visible; patterns can be recorded at beam energies below those at which conventional detectors usefully operate; high precision in cross-correlation based pattern shift measurements needed for high resolution electron backscatter diffraction strain mapping can be obtained. We also show that the physics underlying direct detection is sufficiently well understood at low primary electron energies such that simulated patterns can be generated to verify our experimental data.

DOI: 10.1103/PhysRevLett.111.065506 PACS numbers: 61.05.J−, 07.78.+s, 68.37.Hk

Electron backscatter diffraction (EBSD) is a scanning electron microscope (SEM) based method in which diffraction of low-energy-loss electrons as they exit through the topmost few tens of nanometers leads to Kikuchi diffraction. In most EBSD studies the incident electron beam is stepped across a grid of points on the sample surface and the EBSD patterns analyzed in an automated way to determine crystal phase, orientation, or lattice strain variation. The EBSD method has evolved rapidly over the last two decades [1–5]. Most research has been directed to the application of this versatile tool to an ever increasing array of problems in materials characterization but the analysis methods themselves have also advanced, notably in three dimensional imaging using focused ion beam (FIB)-SEM [6–9] and in strain mapping [10–14]. However, the detector technology used to record EBSD patterns has essentially remained unchanged for over a decade and now limits performance in several application areas, such as strain resolution and low dose mapping, and prevents the development of new areas.

The earliest EBSD patterns were recorded on film either exposed directly to the electrons in the chamber [15–17], or indirectly imaging a phosphor screen using a camera outside the vacuum [18]. Subsequently, these were replaced by various image intensified cameras giving the convenience of a live image of the pattern at the scintillator but with degraded pattern quality compared to that recorded using film [19]. Subsequently, scintillator coupled CCDs were introduced in the early 1990s [20,21]. In a limited number of examples tapered fiber-optic bundles have been used to couple the CCD to the scintillator with good results [20] but the alternative optical lens coupling has been adopted in the vast majority ($>95\%$) of instruments currently in use. Departures from these detection schemes have included an investigation of microchannel plates [22] and the adoption of a retarding electrostatic field for energy filtering [23].

In other fields there have been significant advances in detectors directly exposed to the imaging beam for the detection of x rays [24,25] and medium energy electrons [26–29]. The current development of TEM instruments operating at lower accelerating voltages, largely driven by studies of radiation sensitive carbon-based materials [30], overlaps the detector requirements for EBSD. However, difficulties remain in modeling the detection physics to imaging of low-energy electrons at primary energies typically used for EBSD (5–30 keV).

In this Letter, we report the first detection of EBSD patterns using a directly exposed complementary metal-oxide-semiconductor (CMOS) sensor and demonstrate that the resolution in the patterns is improved compared to those recorded using conventional indirect detectors, particularly at low voltages. A model for the necessary detector physics has also been developed, which enables simulated patterns to be generated for various detector structures and electron budgets.

The direct detector prototype used in our experiments was an active pixel sensor architecture fabricated using a CMOS design (Table I). At the full $\sim$1000 by 1000 pixel camera resolution (desirable for strain mapping) the readout rate of this device is similar to that of commercially available indirect CCD based systems. For orientation mapping the detector readout is often binned down to $\sim$128 by 128 pixels or smaller so that readout at several hundreds of frames per second can be achieved through a reduction in accuracy; however, binning is not possible with this direct detector prototype and the maximum speed is 28 full frames/second.

The CMOS sensor must be back illuminated so that electrons impinge directly into the active layer while avoiding interaction with top passive CMOS layers of the device and thus allowing detection of electrons under typical SEM operating conditions. The sensor was mechanically thinned

 © 2013 American Physical Society

TABLE I. CMOS sensor specifications.

Pixel array	1024×1024
Maximum readout rate	28 full frames/s
Pixel size	$20\ \mu m \times 20\ \mu m$
Dark noise	$27\,e^-$ rms
Analog-digital conversion	12 bits/pixel
Linear dynamic range	$60\,000\,e^-$

and polished to the active layer. The remaining electrically insensitive surface layer at the back of the imager was used as an entry window to match the detector gain with the required dynamic range. For the experiments reported here reactive ion etching was used to reduce the thickness of this entry window further to improve the detective quantum efficiency of low-energy electrons.

The sensor was mounted vertically in the SEM sample chamber in a back illuminated geometry using electrons backscattered from a Si sample tilted by 70° from the incident electron beam. The pattern center was approximately located at the center of the detector. However, due to mechanical constraints the detector was located further away from the sample than is optimal for EBSD and hence subtended a smaller angle of approximately 40° in both vertical and horizontal directions.

A commercially available indirect detector EDAX/TSL Digiview II system was also used under similar conditions to provide reference data. This latter system consisted of an actively cooled CCD device located outside the SEM vacuum chamber imaging a phosphor screen through an f 0.95, 50 mm optical coupling.

To correct for the effects of fixed patterns, dark reference frames were recorded with the beam blanked and bright reference frames were obtained from low magnification scans of a highly deformed region of the aluminium sample stub. Standard dark and bright field corrections were applied in which the dark reference was subtracted from both recorded EBSD patterns and the bright reference and the resultant images were divided for gain normalization. A data set of 100 frames was recorded for each beam position on the sample to enable post-acquisition calculation of EBSD patterns for different effective exposure times.

Figure 1 shows an EBSD pattern obtained from a Si sample using the direct detector with a thick entry window obtained after the mechanical polish, for incident electrons with an energy of 20 keV. A pattern obtained using a similar exposure time using the conventional indirect detector is also shown in Fig. 1 for comparison.

An initial visual comparison indicates that the directly detected pattern is sharper than that obtained with the conventional indirect detector, with high-order features clearly visible. For example, the vertical 220 band in the center of the pattern exhibits both 440 and 660 Kikuchi lines; these are not clearly resolved in the patterns recorded with the indirect detector.

A computational theoretical model has been constructed to simulate the trajectories of the incident electrons on the

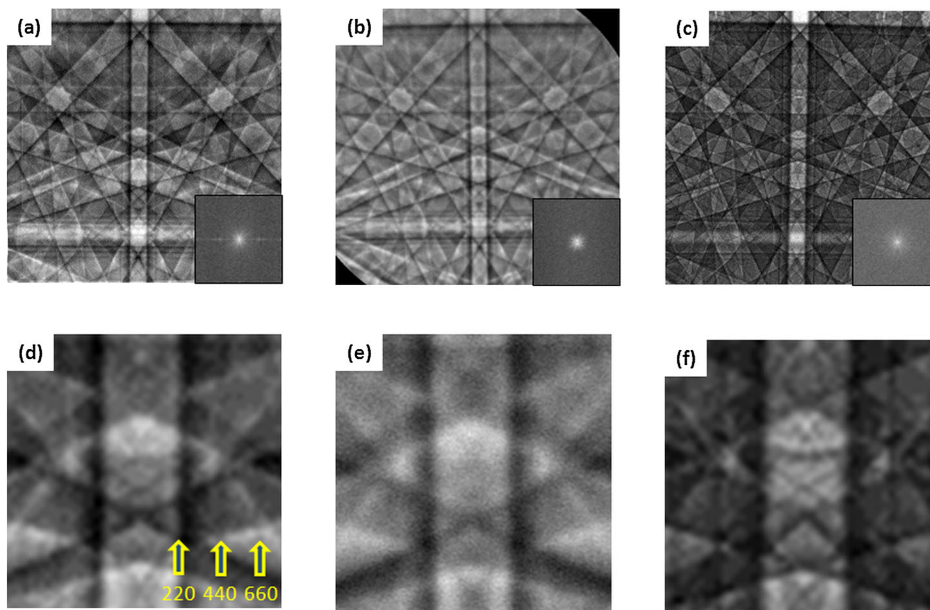

FIG. 1 (color online). EBSD patterns recorded from Si (001) at 20 keV, ~10 nA probe current and 20 s exposure. The bottom right of each pattern (inset) shows the power spectrum obtained from a Fourier transform of a 512×512 pixel region at the center of each image. (a) Direct electron detection and (b) conventional indirect detection. (c) Calculated dynamical diffraction simulation. (d),(e),(f) Enlargement of features near the 114 zone axis. In (a),(d) the vertical 220 band at the center of the pattern exhibits both 440 and 660 Kikuchi lines, the latter often not being visible in (b),(e). Intensities in the extracted 512×512 images were rescaled to zero mean and unit variance before transforming in order to normalize the power spectra.

sensor and the induced signal arising from these, using a modification of previous calculations due to Meyer and Kirkland [31,32]. The charge distribution induced by the incident electrons was calculated using Joy's model [33], which consists of straight electron trajectories between discrete elastic Rutherford scattering events with a continuous energy loss modeled using the Bethe formula along these trajectories. For both the Rutherford and Bethe models relativistic formulations were used and the generation of fast secondary electrons was included [31,32]. The Monte Carlo approach was extended to add thermal noise generated in the sensor and the readout noise arising from the electronics. For these simulations a geometric model of the sensor was constructed including the inactive silicon layer at the back surface, which was estimated to be 1 μm thick after mechanical thinning, reduced to 0.1 μm after plasma etching. Each electron's contribution to the EBSD pattern was simulated, using the calculated image intensity as a probability distribution function, which also provides the Poisson contribution to the noise. The input image intensity was simulated using dynamical diffraction calculations of the Kikuchi band features in EBSD patterns using code developed by Winkelmann [34]. The patterns simulated using this model for the detector geometry, SEM imaging conditions, and for an electron budget corresponding to our experimental data are shown in Fig. 1 demonstrating excellent agreement between simulated and experimental patterns with many subtle, high resolution features in the patterns reproduced in the simulations.

Observations were also made at lower incident electron beam energies. Using a mechanically back thinned device EBSD patterns could be obtained for incident electron energies down to ~10 keV. However, below 10 keV the recorded signal level fell significantly and it was not possible to obtain usable EBSD patterns. However, for the plasma etched device EBSD patterns could be obtained at significantly lower incident beam energies. Figure 2 shows EBSD patterns obtained using 5 keV energy incident electrons, and also compares the performance of the sensor following a mechanical polish with that after plasma etching. For reference EBSD patterns recorded using the conventional indirect detector are also shown. These results clearly illustrate the significant performance benefits of direct detection, particularly at lower incident beam energies. This ability to perform EBSD experiments at lower energies should, in turn, offer significant improvements in spatial resolution.

To quantitatively evaluate the quality of EBSD patterns recorded using direct detection we have measured the precision of pattern shifts induced by movement of the incident electron beam, using cross-correlation methods. These are important as pattern shift measurements form the basis of EBSD strain mapping, which is currently receiving considerable interest [10,14] and as such represents an application where direct detection may have immediate benefits. Patterns were obtained at a series of 7 points spaced by 7 μm in a line scan parallel to the sample tilt axis. At each point 100 frames were recorded with a 200 ms exposure for each frame. Subsequent averaging over different numbers of frames at each position in the line scan has enabled us to explore the effects of different *effective* exposure times (from 0.2 to 20 s) on the pattern

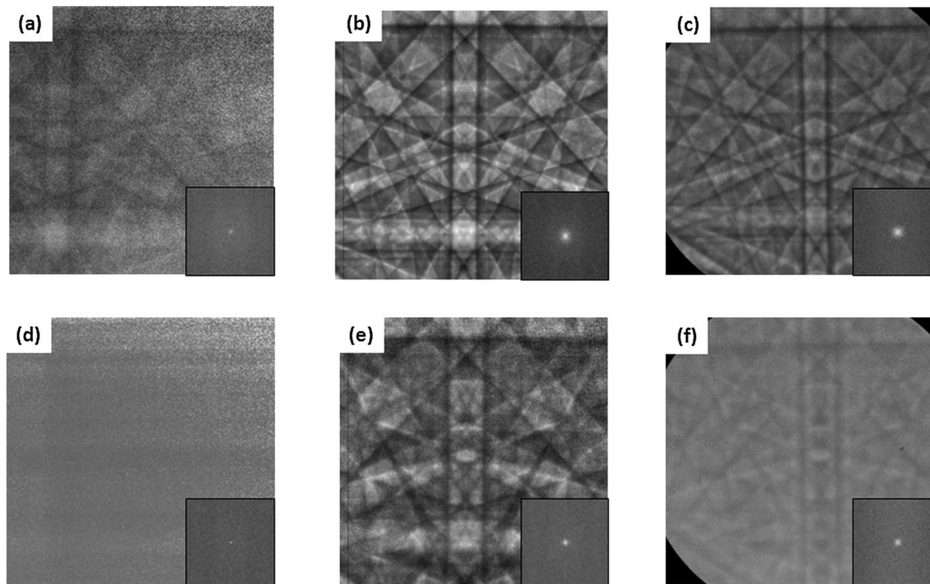

FIG. 2. EBSD patterns from Si (100) recorded by direct electron detection (a),(d) before and (b),(e) after plasma etching, compared to (c),(f) conventional indirect detection. (a),(b),(c),(d),(e) 20 s exposure. (f) 180 s exposure. (a),(b),(c) 10 keV primary energy. (d),(e),(f) 5 keV primary energy. The bottom right of each pattern (inset) shows the power spectrum obtained from a Fourier transform of a 512×512 pixel region at the center of each image.

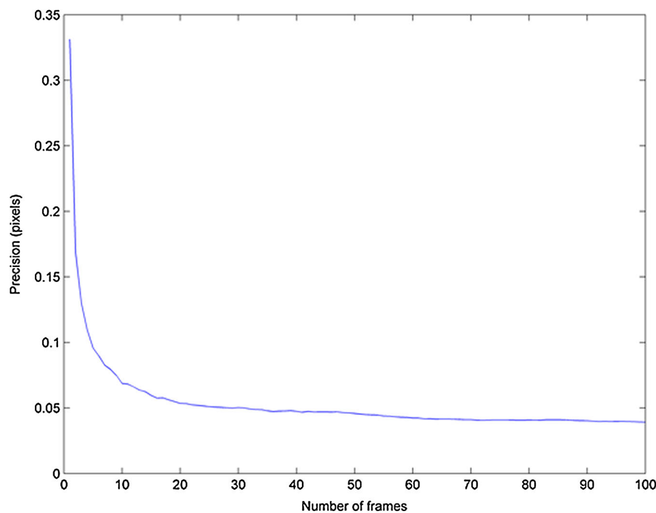

FIG. 3 (color online). Precision of Si (100) EBSD pattern shifts measured between adjacent points on a line scan along the sample tilt axis, as a function of the number of frames averaged. Each frame used a 200 ms exposure and patterns were recorded at 20 keV primary energy with a 9 nA probe current.

shift measurement, with the pattern shift measured for pairs of EBSD patterns obtained from neighboring points in each line scan.

Analysis was performed using a cross-correlation analysis for fifty 256×256 pixel subregions using codes written in MATLAB. For each shift measurement one subregion was located at the center of the image field with nineteen additional subregions located in a ring around the edge of the image field and the remaining thirty subregions placed at random positions. The precision in the shift measurement was evaluated by calculating standard deviations in the measured x and y shift values, for all fifty subregions, averaging these between all pattern pairs, and calculating the Euclidian length in pixels.

Figure 3 shows that, as expected, pattern shift measurements improve as the signal to noise level is increased by averaging over more frames. For long exposure times, the precision in the pattern shift measurements converges to ± 0.038 pixels, corresponding to an angle of $\sim 3 \times 10^{-5}$ rads at the pattern center. This compares favorably to the precision of ± 0.05 pixels ($\sim 8 \times 10^{-5}$ rads) reported for similar measurements using indirect detection [14].

We have presented the first EBSD patterns recorded using direct electron detection in a thin back illuminated CMOS device. These initial observations clearly demonstrate the performance improvements that are possible using direct detection compared to an existing commercially available EBSD detectors based on an indirect scintillator-lens coupled CCD system. This improvement in detector resolution has enabled fine, low-contrast, high-order features to be recorded in the EBSD pattern, which are not visible using the conventional system. In particular, the performance at low incident beam energies is dramatically improved and high quality patterns can be recorded at energies below those at which the conventional detector usefully operates. This ability to operate at low energies is important due to the consequent improvements in spatial resolution and a reduction of sample damage and charging. We have also assessed strain sensitivity using a cross-correlation analysis of pattern shifts and our preliminary results indicate a performance similar or better than conventional detectors. The lack of optical distortion from lens or fiber optic coupling is also a significant added benefit for strain measurement [35].

It is expected that further refinement of the back surface finish of the sensor to further reduce the thickness of the electrically dead layer and an optimization of device pixel size will lead to additional performance improvements surpassing those of indirect EBSD detectors.

This work was supported under EPSRC Grants No. EP/C009509/1 and No. EP/H018921/1 and a European Framework 6 program for an Integrated Infrastructure Initiative 026019 ESTEEM. The authors acknowledge Dr. Thalis Anaxagoras and Prof. Nigel Allinson from the University of Sheffield for provision of CMOS wafers and readout system, and Colin Wilburn of Micron Semiconductor Ltd. for chip packaging.

*Current address: Oxford Instruments, Halifax Road, High Wycombe HP12 3SE, United Kingdom.

[1] D. Dingley, J. Microsc. **213**, 214 (2004).
[2] F. J. Humphreys, J. Mater. Sci. **36**, 3833 (2001).
[3] V. Randle, Mater. Charact. **60**, 913 (2009).
[4] A. J. Wilkinson and P. B. Hirsch, Micron **28**, 279 (1997).
[5] M. U. Farooq, R. Villaurrutia, I. MacLaren, T. L. Burnett, T. P. Comyn, A. J. Bell, H. Kungl, and M. J. Hoffmann, J. Appl. Phys. **104**, 024111 (2008).
[6] D. J. Child, G. D. West, and R. C. Thomson, Ultramicroscopy **114**, 1 (2012).
[7] M. A. Groeber, B. K. Haley, M. D. Uchic, D. M. Dimiduk, and S. Ghosh, Mater. Charact. **57**, 259 (2006).
[8] M. Uchic, M. Groeber, M. Shah, A. Shiveley, and J. Spowart, Microsc. Microanal. **17**, 988 (2011).
[9] N. Zaafarani, D. Raabe, R. N. Singh, F. Roters, and S. Zaefferer, Acta Mater. **54**, 1863 (2006).
[10] T. B. Britton and A. J. Wilkinson, Ultramicroscopy **114**, 82 (2012).
[11] C. Trager-Cowan, F. Sweeney, P. W. Trimby, A. P. Day, A. Gholinia, N. H. Schmidt, P. J. Parbrook, A. J. Wilkinson, and I. M. Watson, Phys. Rev. B **75**, 085301 (2007).
[12] A. J. Wilkinson, G. Meaden, and D. J. Dingley, Superlattices Microstruct. **45**, 285 (2009).
[13] A. J. Wilkinson, J. Electron Microsc. **49**, 299 (2000).
[14] A. J. Wilkinson, G. Meaden, and D. J. Dingley, Ultramicroscopy **106**, 307 (2006).
[15] D. J. Dingley, K. Z. Baba-Kishi, and V. Randle, *Atlas of Backscattering Kikuchi Diffraction Patterns* (Institute of Physics, Bristol, 1995).

[16] J. A. Venables and C. J. Harland, Philos. Mag. **27**, 1193 (1973).
[17] A. J. Wilkinson and D. J. Dingley, Acta Metall. Mater. **40**, 3357 (1992).
[18] J. A. Venables and R. bin-Jaya, Philos. Mag. **35**, 1317 (1977).
[19] D. J. Dingley, M. Longden, J. Weinbren, and J. Alderman, Scanning Microsc. **1**, 451 (1987).
[20] R. P. Goehner and J. R. Michael, J. Res. Natl. Inst. Stand. Technol. **101**, 301 (1996).
[21] J. R. Michael and R. P. Goehner, *Proceedings of the Fifty-Second Annual Meeting of the Microscopy Society of America* (San Francisco Press, San Francisco, 1994), p 596.
[22] D. L. Barr and W. L. Brown, Rev. Sci. Instrum. **66**, 3480 (1995).
[23] A. Deal, T. Hooghan, and A. Eades, Ultramicroscopy **108**, 116 (2008).
[24] M. Battaglia, D. Bisello, R. Celestre, D. Contarato, P. Denes, S. Mattiazzo, and C. Tindall, Nucl. Instrum. Methods Phys. Res., Sect. A **674**, 51 (2012).
[25] R. Turchetta *et al.*, Nucl. Instrum. Methods Phys. Res., Sect. A **458**, 677 (2001).
[26] M. Battaglia, D. Contarato, P. Denes, D. Doering, T. Duden, B. Krieger, P. Giubilato, D. Gnani, and V. Radmilovic, Nucl. Instrum. Methods Phys. Res., Sect. A **622**, 669 (2010).
[27] D. Contarato, P. Denes, D. Doering, J. Joseph, and B. Krieger, Nucl. Instrum. Methods Phys. Res., Sect. A **635**, 69 (2011).
[28] N. Guerrini, R. Turchetta, G. Van Hoften, R. Henderson, G. McMullan, and A. R. Faruqi, JINST **6**, C03003 (2011).
[29] A. C. Milazzo, G. Moldovan, J. Lanman, L. Jin, J. C. Bouwer, S. Klienfelder, S. T. Peltier, M. H. Ellisman, A. I. Kirkland, and N.-H. Xuong, Ultramicroscopy **110**, 741 (2010).
[30] U. Kaiser *et al.*, Ultramicroscopy **111**, 1239 (2011).
[31] R. R. Meyer and A. I. Kirkland, Microsc. Res. Tech. **49**, 269 (2000).
[32] R. R. Meyer and A. I. Kirkland, Ultramicroscopy **75**, 23 (1998).
[33] D. C. Joy, *Monte Carlo Modelling for Electron Microscopy and Microanalysis* (Oxford University Press, Oxford, 1995).
[34] A. Winkelmann, C. Trager-Cowan, F. Sweeney, A. P. Day, and P. Parbrook, Ultramicroscopy **107**, 414 (2007).
[35] T. B. Britton, C. Maurice, R. Fortunier, J. H. Driver, A. P. Day, G. Meaden, D. J. Dingley, K. Mingard, and A. J. Wilkinson, Ultramicroscopy **110**, 1443 (2010).